

## Evolution of the initial hole in vertically vibrated shear thickening fluids

Yulei Xu,<sup>1</sup> Xinglong Gong,<sup>1,\*</sup> Yingqiang Sun,<sup>2</sup> Shouhu Xuan,<sup>1</sup> Wanquan Jiang,<sup>2</sup> and Zhong Zhang<sup>3</sup>

<sup>1</sup>*CAS Key Laboratory of Mechanical Behavior and Design of Materials, Department of Modern Mechanics, University of Science and Technology of China, Hefei 230027, China*

<sup>2</sup>*Department of Chemistry, University of Science and Technology of China, Hefei 230026, China*

<sup>3</sup>*National Center for Nanoscience and Technology, Beijing 100080, China*

(Received 22 October 2010; revised manuscript received 19 January 2011; published 11 May 2011)

The apparent viscosity of shear thickening fluid (STF) changes dramatically with the applied shear rate, which is a typical rheological property of STF. Such a rheological property affects the vertically vibrated dynamic property of STF. In order to get a better understanding of the vertically vibrated dynamic properties of STF, the surface instabilities in vertically vibrated STF, which was prepared by suspending polymethylmethacrylate particles in ethylene glycol, are investigated. Above a critical driving acceleration, the surface instability transforms from the disappearance to the fission of the initial hole, which is produced by applying a finite perturbation to the surface. The time required for the initial hole to disappear can be affected by the driving acceleration, vibration frequency, volume fraction, thickness, and shape and size of the perturbation. A possible model is proposed, and the expressions of hydrostatic force and viscous dissipative force are employed to clarify the relationship between disappearance of the hole and shear thickening effect. The fission and spreading follow a hexagonal arrangement. At a higher acceleration, the holes cover the entire surface in a state of disorder. The mechanism for the initial hole's evolution in vertically vibrated shear thickening fluids is discussed.

DOI: [10.1103/PhysRevE.83.056311](https://doi.org/10.1103/PhysRevE.83.056311)

PACS number(s): 47.57.-s, 45.70.-n

### I. INTRODUCTION

Shear thickening fluid (STF) is a kind of particulate suspension whose rheological property takes place as an abrupt change when encountering a strike. The apparent viscosity of STF changes so dramatically at a high-speed impact that it may transform from a suspension to a solid-like status. The viscosity comes back rapidly when the impact is removed, which indicates that the shear thickening effect is a reversible non-Newtonian behavior. The rheological properties of these STFs have been carefully investigated under steady and dynamical rheological measurements. Various theoretical and experimental methods have been developed to study their shear thickening effects [1–9]. Recently, surface instabilities and pattern transformations of STFs have gradually been the new focus of research [10,11]. Some of these instabilities are similar to those in Newtonian fluids and other non-Newtonian fluids, while others are not.

The surface of a free fluid without any disturbance is perpendicular to the direction of gravity. When a hole was poked into the surface, it will be fully filled immediately by the surrounding fluids because of hydrodynamic pressure. Such a surface transformation, which is often defined as surface instability, is highly dependent on the vertically vibrated dynamic property of the fluid. During the last few decades, the surface morphologies for the vertically vibrated fluids have been extensively investigated [12], and many interesting phenomena such as Faraday waves [13], Rayleigh-Taylor instability [14], and oscillons [15] have been found. The vertically vibrated suspensions, which are composed of particle-dispersion fluid, also show those instabilities. The Faraday wave is observed in wormlike micelles [16], while the oscillons and solitary waves are found in a clay suspension [17]. Convective heaps resulting from Rayleigh-Taylor instability appear in granular

slurries [18]. To better understand the vertically vibrated dynamic properties of STFs, study of their surface instabilities is necessary.

The surface instabilities have usually been investigated by applying a perturbation that produced a localized hole in vertically vibrated shear thickening suspensions. The surface instabilities could be characterized by investigating the evolution of the initial hole. Recently, Merkt *et al.* [10] found that persistent holes were created by localized perturbation in cornstarch or glass microsphere suspensions despite the hydrodynamic pressure of the surrounding fluids. These holes can persist while the vibration acceleration is above a certain threshold, and they immediately disappear upon the cessation of vibration. On their observations they predicated that the stability of the holes was attributed to shear thickening. Deegan [19] showed that a hysteretic stress-strain rate relation played a key role in the stability of persistent holes. Ebata *et al.* [11] found that in dense glass bead suspensions, such a hole gradually expanded until it collided with the side wall of the container rather than just persisting when the glass beads were larger than a certain size. The convection-like flow [20] at the rim sustained the expanding hole. The onset conditions and detailed dynamics of expanding holes were also investigated. They indicated that viscous stress played an important role and conjectured that the connection between dynamics and rheological properties could be used to elucidate the mechanism. Epstein and Deegan [21] observed strip waves in vibrated shear thickening wormlike micellar solutions and found that the rheological properties of the fluid accounted for the formation of strip waves. To date, the investigation of vertically vibrated STF is still in an early stage, and the theory and experiment are both far from perfect. Therefore, more research on the vertically vibrated STF needs to be done.

Here we present the results of our study on vertically vibrated STF with polymethylmethacrylate (PMMA) particles suspended in ethylene glycol. The suspensions reveal obvious shear thickening rheological properties, and their viscosity is shear rate dependent. To fully understand their vertically

\*gongxl@ustc.edu.cn

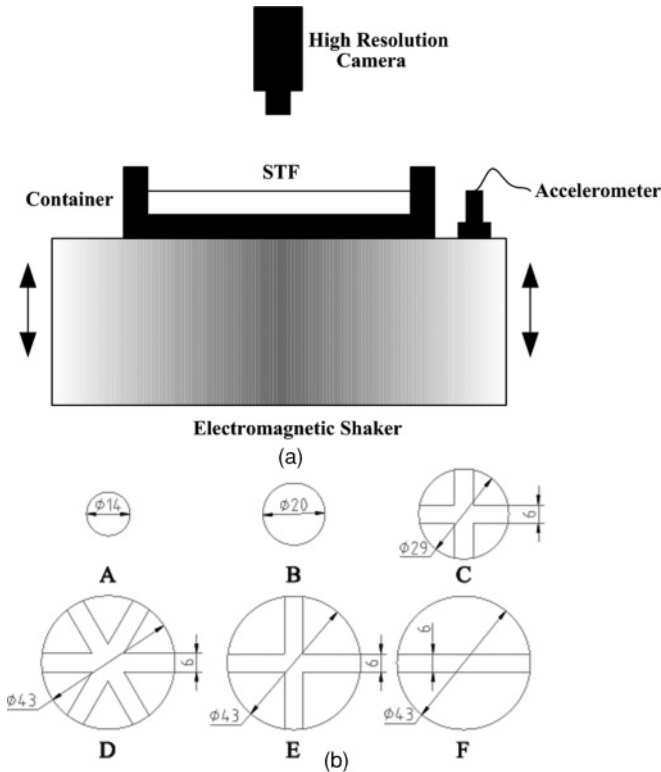


FIG. 1. (a) Sketch of the experimental apparatus used for vertically vibration. (b) The morphology of rubber plugs producing initial perturbations.

vibrated dynamic property, the surface instability of the vertically vibrated STF is systematically studied. When the acceleration exceeds a certain threshold, our system displays an ordered fission of the perturbation, which spreads and arranges in hexagonal structure chains, a result that is different from the previous reports. Different shapes and sizes of the initial perturbation are also discussed. The onset conditions and evolution of ordered hexagonal fissions are investigated. When the acceleration is below a certain threshold, the perturbation disappears gradually. As the acceleration increases to a critical value above a certain threshold, the disorder state emerges. The evolutions before and after the ordered fission are studied in detail. The factors affecting the disappearing time of the initial hole and the convection-like flow at the rim of the hole are also investigated systematically.

## II. MATERIALS AND METHODS

A soap-free emulsion polymerization method was used to prepare the PMMA particles [22]. Then the PMMA particles were suspended in ethylene glycol to form the STF mixture. The volume fraction of the system  $\phi$  was varied from 50% to 60%. The mixture was placed in a ball mill grinding up to about 24 hours. The STF samples were treated in a vacuum for 2 hours in order to exclude the bubbles.

The morphology of the PMMA particles was characterized by scanning electron microscope (SEM) (JEOL, type JSM-6700F). The PMMA particles are spherical and in good monodispersity. The average size was about  $2.5 \mu\text{m}$ . In the vertically vibrated experiments, the experimental apparatus, as

shown in Fig. 1(a), consists of an aluminum container mounted on an electromagnetic shaker (DY-300-2). The container is an aluminum column with its inner diameter 109 mm, and the suspension layer depth varied from 2 to 5 mm. The container was vertically oscillated sinusoidally with an acceleration amplitude  $a$  from 0 to  $290 \text{ m s}^{-2}$  and a frequency  $f$  from 40 to 80 Hz. Six kinds of rubber plugs with different shapes and sizes were illustrated in Fig. 1(b). The local initial perturbation was created by making a marking in the flat surface with a rubber plug, and the evolution of the hole was recorded by a high-resolution camera. Rheological properties [23,24] were measured by using a rheometer (Anton Paar, Physica MCR301) with a cone plate of angle  $2.007^\circ$  and diameter 24.967 mm. The strain varied from 0.1 to 2, and the shear rate varied from 1 to  $100 \text{ s}^{-1}$ . All the experiments were conducted at the room temperature.

## III. RESULTS AND DISCUSSIONS

### A. General hole evolution

In the previous work, the rheological properties of the silica-based STF sample have been studied systematically [25]. Because the STF sample with softer PMMA particles has a lower critical value than the one with harder silica [26], the apparent properties of the STF sample with PMMA particles can more easily be observed. Here the STF sample with PMMA particles is adopted in the vertically vibrated experiments. The evolution of the initial hole with the increase of the forcing acceleration and time in vertically vibrated STF is investigated in detail by varying the frequency, volume fraction, thickness, and shape and size of the initial hole.

In the vertically vibrated experiments, for the STF samples with lower volume fraction, such as 50% and 52%, the initial

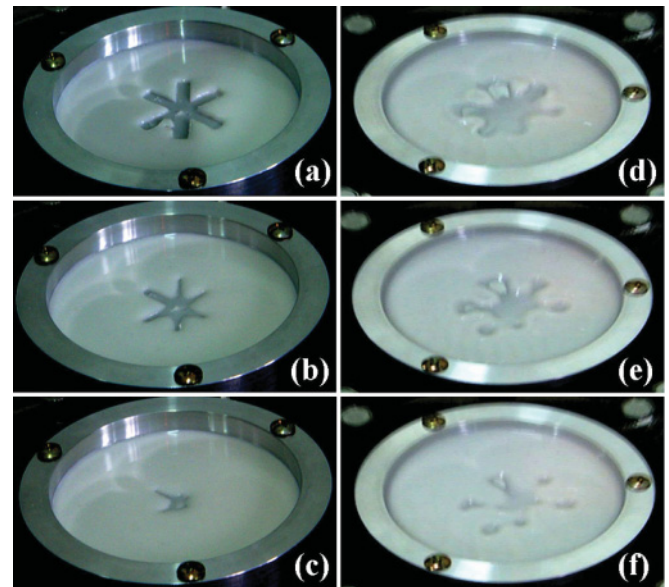


FIG. 2. (Color online) Time evolution of the initial hole produced by rubber plug D for sample with the volume fraction 60% at 40 Hz. Disappearance of the hole:  $a = 25 \text{ m s}^{-2}$ , (a)  $t = 0 \text{ s}$ , (b)  $t = 3 \text{ s}$ , (c)  $t = 10 \text{ s}$ ; fission of the hole:  $a = 225 \text{ m s}^{-2}$ , (d)  $t = 0 \text{ s}$ , (e)  $t = 7 \text{ s}$ , (f)  $t = 15 \text{ s}$ .

hole disappears gradually (data not shown in Fig. 2). The time required to disappear at a higher acceleration is longer than that at a lower acceleration. For the higher volume fraction (60%), the initial hole disappears gradually at the low acceleration. Similar to the lower volume fraction sample, the higher the acceleration is, the longer the time required for disappearing is. Interestingly, when the acceleration reaches a critical threshold ( $225 \text{ m s}^{-2}$  for 40 Hz), the initial hole is divided into small holes (see Fig. 2), and the small holes continue dividing and spreading. Figure 2(a)–2(c) gives the photographs of the hole evolution at low acceleration. It is found that the initial hole produced by rubber plug D shrinks to a small hole gradually and finally disappears. Figure 2(d)–2(f) shows the prime evolution of the initial hole at a high acceleration above the threshold. The initial hole shrinks to several small holes [Fig. 2(f)] rather than one small hole in the center, and then these small holes continue dividing and spreading (data not shown in Fig. 2). After a long period of equilibrium, these small holes tend to be uniform. In this case, the small holes are arranged in hexagonal patterns. With further increasing acceleration, the fission of the holes becomes drastic, and the average size of the hole is diminished. If the acceleration is increased above an extreme value ( $290 \text{ m s}^{-2}$  for 40 Hz), whether the initial hole is present or not, new holes will be produced in the surface. These holes are randomly arranged, and the surface of STF suspension is disordered. In our work, by varying the acceleration, the overall surface instability can be divided into three parts: disappearance of the hole, fission of the hole, and disorder state.

Figure 3(a) shows the primary stage after the introduction of an initial hole into the vertically vibrated shear thickening suspensions. The evolution of the initial hole could be observed with the increasing time. Different kinds of hole evolution will be obtained under different acceleration. This phenomenon should respond to the convection-like flow at the rim of the initial hole, which is caused by the shear thickening effect resulting from the shear rate dependence of microstructures [25].

Due to the high concentration and the fine monodispersity of particles, there is a close-packed hexagonal layer structure of particles in dense suspension [shown at the right of Fig. 3(b)]. When the acceleration is very low, the shear rate applied on the suspension and the acting force on the particle are very small. The force is so small that the offset of particle does not occur, and the microstructure of suspension does not change distinctively. Accordingly, no obvious change is observed for the viscosity, which is similar to the Newtonian fluid. The hole poked in the suspension surface will soon be filled by the surrounding fluids because of hydrodynamic pressure [left side of Fig. 3(b)]. With increasing forcing acceleration, the shear rate applying on the suspension at the rim of the initial hole also increases. The particles at the rim of the initial hole begin to move away, and the ordered structure begins to be destroyed. Then the particle aggregations are formed [shown at the right of Fig. 3(c)]. Therefore, the viscosity of the suspension increases at the rim of the initial hole. Here a convection-like flow, which can resist the hydrodynamic pressure of the surrounding fluids, is obtained. As a result the disappearing time for the initial hole increases. With further increasing of the forcing acceleration, the shear rate at the

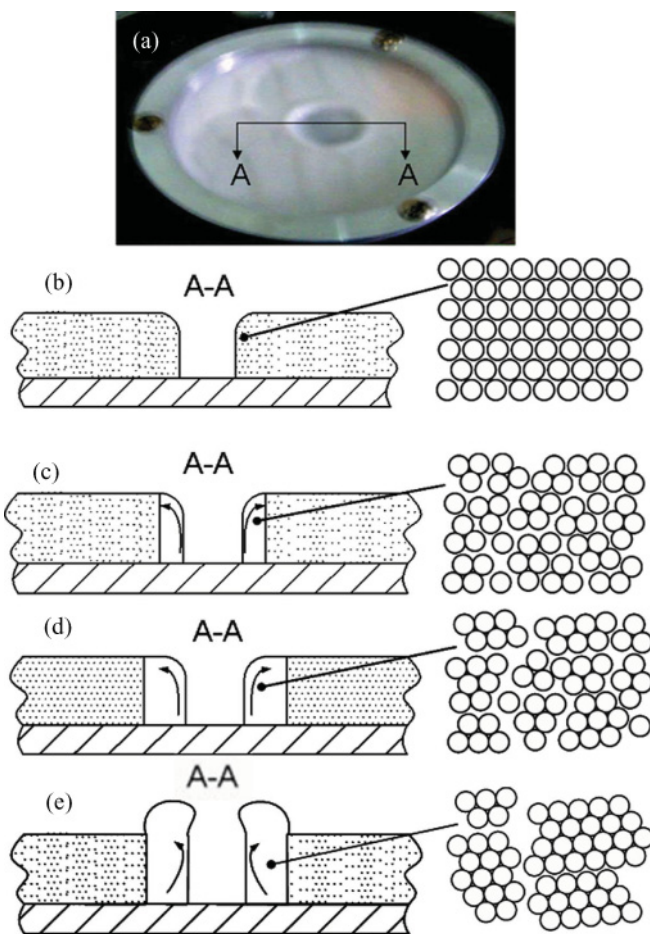


FIG. 3. (Color online) Schematic cross section and microstructure of the rim of the initial hole at different acceleration during the evolution of the initial hole. (a) Initial state of a localized hole in vertically vibrated shear thickening suspensions which indicates the position of the cross section; (b) at very low acceleration; (c) at intermediate acceleration; (d) at relatively high acceleration; (e) above a certain critical acceleration ( $225 \text{ m s}^{-2}$  for 40 Hz).

rim of the initial hole also increases. The particle aggregations become intense, and the particle clusters are formed [shown at the right of Fig. 3(d)]. Accordingly, the viscosity of suspension at the rim of the initial hole increases. To this end, the resulting convection-like flow becomes severe [shown at the left of Fig. 3(d)], and the resistance to the hydrodynamic pressure becomes strong. Therefore, more time is needed for the hole to disappear.

When the acceleration reaches to a critical value ( $225 \text{ m s}^{-2}$  for 40 Hz), the increasing shear rate induces the particle clusters to be larger [shown at the right of Fig. 3(e)] and the viscosity to be higher. Correspondingly, the convection-like flow is strong enough to resist the hydrodynamic pressure, which further leads to the nondisappearance of the initial hole. During the resistance to the hydrodynamic pressure, the convection-like flow piles up, and the upper surface of the STF at the rim of the initial hole rises continuously [shown at the left of Fig. 3(e)]. Above a certain height, parts of the convection-like rim fall into the central hole, and then these parts either separate the central hole into small holes or disappear at the bottom. The former case leads to the

fission of the initial hole. In previous reports, the average size of the particles used for the suspension is 20  $\mu\text{m}$ , and the area of convection-like flow is powerful enough and in balance with the hydrodynamic pressure. Thus the initial hole is persistent [10]. When the particles increase to 200  $\mu\text{m}$ , however, the convection-like flow defeats the hydrodynamic pressure. The hole begins to expand rather than disappear [11]. In this paper the size of the particles is only 2.5  $\mu\text{m}$ ; thus the convection-like flow leads to the fission of the initial hole as discussed above.

When the acceleration is larger than an extreme value (290  $\text{m s}^{-2}$  for 40 Hz), the shear rate applying on suspension and the acting force on the particle clusters are large enough to tear the particle clusters, which results in many small holes. Then the suspension is in a disorder state. Overall, the transformation of the convection-like flow at the rim of the hole could be employed to explain the evolution of the initial hole in vertically vibrated shear thickening fluids. Further theoretical and modeling work will be done in detail.

Regardless of the sample thickness, the evolution of the initial hole would go through these three process by varying the acceleration: disappearance of the hole, fission of the hole, and disorder state. Figure 4 gives the phase diagram for samples with different thicknesses. In the phase diagram, the onset acceleration for the fission of the hole decreases monotonically with the increasing of the sample thickness. The reason for the initial hole's fission is illustrated in Fig. 3(e). Parts of the convection-like rim falls into the central hole; thus the central hole would be separated into small holes. When the height of the convection-like rim increases above a certain value and the convection-like rim becomes unstable, parts of the convection-like rim would fall into the central hole. Hence, with the increasing sample thickness, the convection-like rim becomes more unstable. In consequence, the onset acceleration for the fission of the hole is in inverse proportion to the sample thickness. From Fig. 4 it also can be seen that the onset acceleration for the disorder state changes little with

the increasing sample thickness. In the disorder state, many small holes that appeared due to the particle clusters were destroyed. Only when the shear rate applying on suspension and the acting force on the particle clusters are large enough could the particle clusters be separated. Therefore, the onset of disorder state is dependent on the shear rate but not the sample thickness.

### B. Disappearance of the hole

If the volume fraction of the suspension is low enough, the initial hole disappears gradually despite the acceleration varying from 0 to 300  $\text{m s}^{-2}$ , which is the range of the acceleration that could be supplied by our instrument. When the volume fraction exceeds a critical value, the evolution of the initial hole varies by varying the acceleration. The low acceleration often leads to the disappearance of the initial hole. Here the time required for the disappearance of the initial hole is affected by many factors, such as the acceleration, frequency, volume fraction, thickness, shape and size of the initial hole, and so on.

Previously, a reduced one-dimensional model of hydrodynamics was supplied to study the vertically vibrated dynamics of suspensions [19]. Based on this work, a possible model is proposed to better understand the disappearance of the hole. During the disappearance of the initial hole, no observable exchange between the rim of the hole and the other surrounding fluid occurs. As a result, the rim of the hole could be regarded as a rigid mass (shown as the dashed part in Fig. 5). Because of the axial symmetry, only the right side is considered. In the horizontal direction, the rigid mass is under the action of the hydrostatic force  $F_h$  (leftward) and the viscous dissipative force  $F_v$  (rightward). The horizontal hydrostatic force is

$$F_h = L \int_0^h \rho(a \sin \omega t - g)(h - y) dy = \frac{1}{2} \rho L (a \sin \omega t - g) h^2.$$

In this equation,  $L$  is the rigid mass's length, which is perpendicular to the cross section,  $\rho$  is the sample's density,  $h$  is the sample's thickness,  $g$  is acceleration of gravity, and  $a \sin \omega t - g$  is the total acceleration. The viscous dissipative force is related to the shear rate, and the shear rate is related to the horizontal velocity of the rigid mass. Hence, the viscous dissipative force should be assumed to be  $F_v = F(\dot{X}, t) \dot{X}$ . The rate of energy loss could be equivalent to the rate of work due to the viscous dissipative force, and the viscous dissipative force is  $F_v = \frac{\eta V}{H^2} \dot{X}$ , where  $\eta$  is the sample's viscosity, which changes with the shear rate.  $V$  is the volume of the rigid mass.

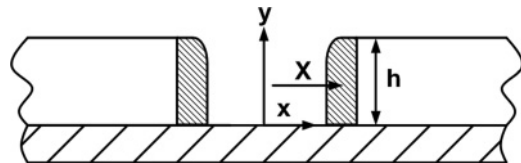


FIG. 5. Schematic cross-sectional model for the disappearance of the initial hole. The dashed part at the rim of the initial hole is regarded as a rigid mass.  $X$  represents the distance of the rigid body's mass center apart from the center, and  $h$  represents the sample thickness.

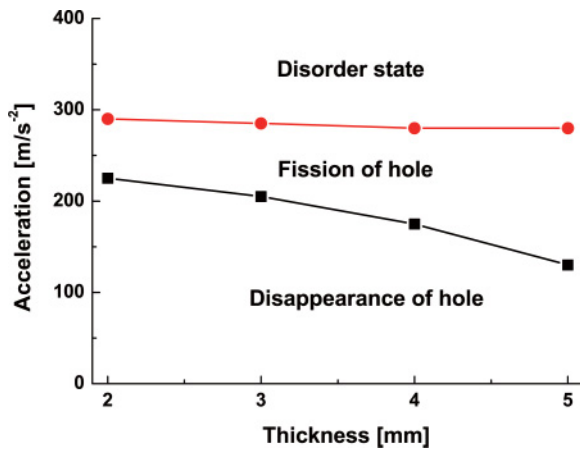


FIG. 4. (Color online) Phase diagram for sample with the volume fraction 60% at 40 Hz, shown as acceleration versus sample thickness. Circles (red) represent the frontier between the fission of the hole region and the disorder state region. Squares (black) represent the frontier between the disappearance of the hole region and the fission of the hole region.

$H$  is defined as  $H \equiv \frac{\dot{X}}{\gamma}$ , whose unit is the length. According to the definition of shear rate, it is a gradient of velocity in a flowing material, and consequently the parameter  $H$  is of the order of the sample's thickness. When the sample's thickness  $h$  increases,  $H$  increases. Here the sample's thickness is postulated to be constant, because the hole area is much smaller than the total area and the change of thickness is neglected. Therefore,  $H$  is regarded as a constant during the following derivation. Based on Newton's second law, the balanced equation could be obtained,  $\rho V \ddot{X} = F_h - F_v$ . In terms of the horizontal hydrostatic force's and viscous dissipative force's expressions, the balanced equation is transformed into

$$\rho V \ddot{X} = \frac{1}{2} \rho L (a \sin \omega t - g) h^2 - \frac{\eta V}{H^2} \dot{X}.$$

Through solving this equation, the viscous dissipative force can be derived:

$$F_v = \frac{1}{2} \rho L (a \sin \omega t - g) h^2 \left( 1 - e^{-\frac{\eta}{\rho H^2} t} \right),$$

which could be simplified as  $F_v = F_h (1 - e^{-\frac{\eta}{\rho H^2} t})$ .

From the expression of viscous dissipative force, it is found that the viscous dissipative force is always smaller than the hydrostatic force during the disappearance of the hole. The hole gradually disappears under the action of the hydrostatic force and the viscous dissipative force. The shear thickening effect often leads to the increase of the sample's viscosity. Considering the expression of viscous dissipative force, with increasing viscosity, the viscous dissipative force increases, and the viscous dissipative force approaches the hydrostatic force progressively. Correspondingly, more time is needed for the hole's disappearance.

The vertically vibrated acceleration plays an important role for the disappearing time. As shown in Fig. 6(b), the shear thickening behavior can be fitted by the power-law function,  $\tau = k \dot{\gamma}^n$  ( $n > 1$ ). In this equation,  $n$  symbolizes a non-Newtonian exponent. The higher the value of  $n$  is, the more obvious the non-Newtonian behavior is. When  $n = 1$ , it represents a typical Newtonian fluid. By minimizing errors between experimental results and model-predicting values, the two parameters  $k$  and  $n$  can be identified. Then the modeling-prediction data can be reconstructed. Figure 6(b) shows the comparison between experimental results and model-predicted values. Obviously, the experimental data of shear stress versus shear rate are essentially in accordance with the theoretical rheological fitting curve of STF. The relationship between viscosity and shear rate is  $\eta = \frac{\tau}{\dot{\gamma}} = k \dot{\gamma}^{n-1}$ . (As the shear rate approaches zero, the viscosity cannot vanish, and there is zero field viscosity. Our work focused on the study of viscosity that is obtained above the limitation of the shear rate. This equation is applicable in the range of our discussion.). The shear rate is in direct proportion to the horizontal velocity  $\dot{X}$ , and the horizontal velocity is in direct proportion to

$$F_v / \frac{\eta V}{H^2} = \left[ \frac{1}{2} \rho L (a \sin \omega t - g) h^2 (1 - e^{-\frac{\eta}{\rho H^2} t}) \right] / \frac{\eta V}{H^2}.$$

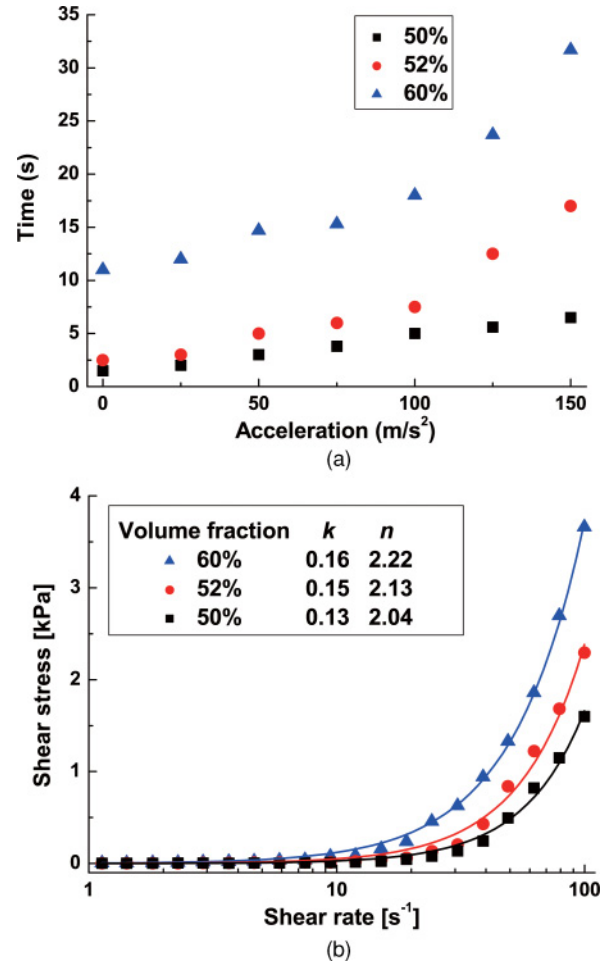


FIG. 6. (Color online) (a) Time required to disappear for the initial hole produced by rubber plug A versus acceleration for sample with three different volume fractions at 40 Hz. (b) Shear stress versus shear rate for the same samples. The solid points represent the experimental data, and the curve represents the theoretical power-law curve.

From this equation, it can be known that horizontal velocity is in direct proportion to acceleration. As a result, the shear rate increases with increasing acceleration. Correspondingly, the sample's viscosity increases and the disappearing time becomes longer, which is in good agreement with the vertically vibrated experiment. As shown in Fig. 6(a), the disappearing time is in proportion to the vertically vibrated acceleration at a constant frequency. With increasing acceleration, the time increases. For an ordinary fluid, the time is very short, and for an ordinary solid, the time is infinite long. In other words, when the acceleration increases, the STF sample transforms from the fluidlike state to the solid-like state, and this phenomenon indicates that shear thickening effect occurs.

Besides the acceleration, the volume fraction of the STF sample is also a key influencing factor. Figure 6(a) indicates that the volume fraction of the STF sample affects the disappearing time markedly. At a same acceleration, the disappearing time increases with increasing of the volume fraction, which is due to the enhancement of the shear thickening effect with a high volume fraction. According to Fig. 6(b), fitting parameters  $k$  and  $n$  of STF samples with

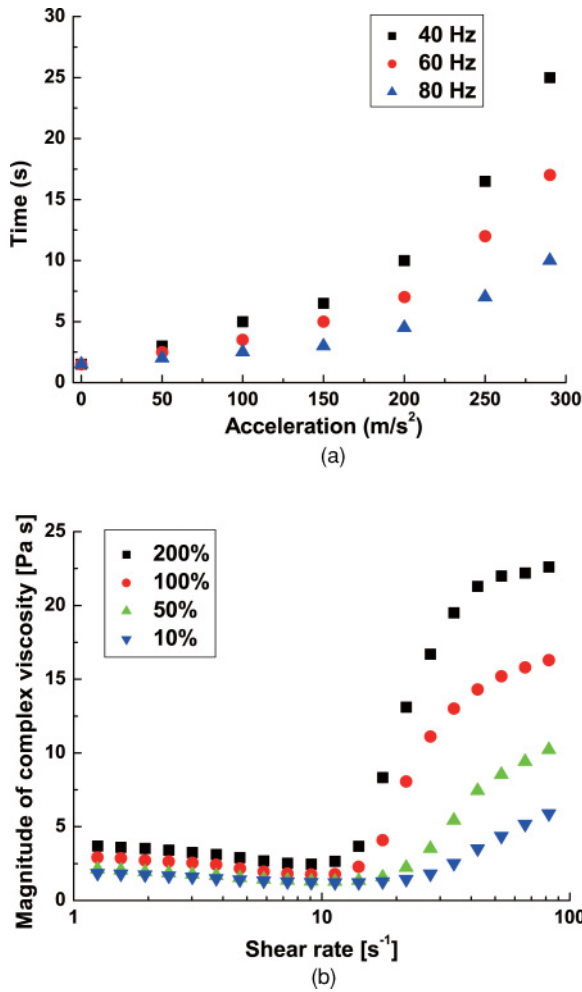


FIG. 7. (Color online) (a) Time required to disappear for the initial hole produced by rubber plug A versus acceleration for sample with the volume fraction 50% at three different frequencies. (b) Magnitude of complex viscosity versus shear rate for the same sample at different strain.

different volume fractions could be obtained and are listed. For different volume fractions, the fitting parameters  $k$  and  $n$  are different. As expected,  $n$  increases with increasing of the volume fraction. If the volume fraction is large, non-Newtonian behavior is obvious, and the shear thickening effect is strong, which further lead to the increasing viscosity and the disappearing time. Therefore, in the vertically vibrated experiment, the persistent time for the initial hole becomes long with increasing the volume fraction.

Figure 7(a) shows the influence of frequency on the disappearing time. At the same acceleration, the higher the frequency is, the shorter the time is. Generally, besides the shear thickening effect, the STF sample also shows the strain thickening effect. Figure 7(b) shows the strain thickening effect of the STF sample. If the shear rate is kept constant, sample's viscosity increases with increasing strain. Moreover, when the shear rate is high, the increase of viscosity with increasing strain is large. Therefore, if the acceleration maintains a same value, the vertically vibrated displacement amplitude is inversely proportional to the frequency [Fig. 7(a)]. The increases of frequency often lead to the decreases of the

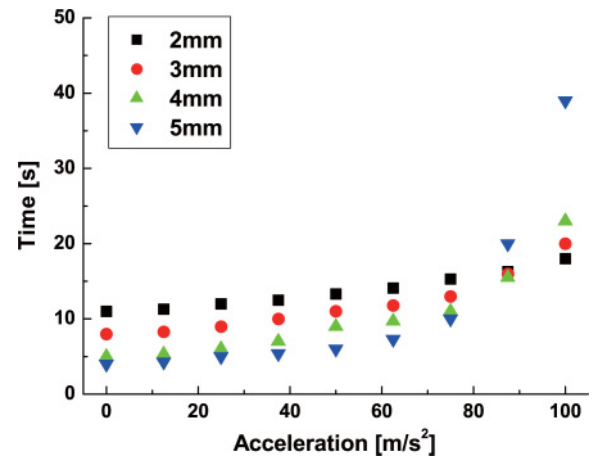


FIG. 8. (Color online) Disappearing time for the initial hole produced by rubber plug A versus acceleration for sample of different thickness with the volume fraction 60% at 40 Hz.

displacement amplitude and the strain applied to the STF sample, respectively. As a result, the sample's viscosity decreases. According to the expression of the viscous dissipative force, the disappearing time gets longer due to the increase of sample's viscosity. Moreover, if the acceleration is high, the change of the viscosity and the disappearing time becomes quicker with increasing frequency. In general, the disappearing time is inversely proportion to the vertically vibrated frequency in the same condition.

Figure 8 shows the relationship between the disappearing time and the acceleration (frequency 40 Hz) under different sample thicknesses. The disappearing time decreases with increasing the sample thickness at a relative low acceleration. As discussed in Fig. 3, when the acceleration is low, the viscous dissipative force is relatively small due to the low viscosity. Thus, the hydrodynamic pressure plays a dominant role. The hydrostatic force,  $F_h = \frac{1}{2}\rho L(a \sin \omega t - g)h^2$ , is in direct proportion to the sample thickness. Due to the presence of the hydrodynamic pressure of surrounding fluids, the initial hole will soon disappear. With increasing the sample thickness, the disappearing time is shortened because of the increasing hydrodynamic pressure. However, under a relative high acceleration, the disappearing time increases remarkably with increasing sample thickness. This is probably because of the enhancement of convection-like flow at the rim of the initial hole. When the acceleration is relatively high, the shear rate becomes large and the particles aggregate to large particle clusters. The viscosity at the rim of the initial hole is increased and the resulting convection-like flow is enhanced, and then the disappearing time increases as mentioned in Sec. IIIA. The resistance of convection-like flow is mainly contribution to the viscous dissipative force. With increasing the sample thickness,  $H$  increases and the enhancement trend of the severe convection-like flow outstrips the hydrodynamic pressure. As a result, the disappearing time is prolonged with increasing sample thickness at a high acceleration.

The influences of the shape and size of the initial hole on the disappearing time are shown in Fig. 9, and the parameters of rubber plug A to F are found in Fig. 1(b). In order to isolate

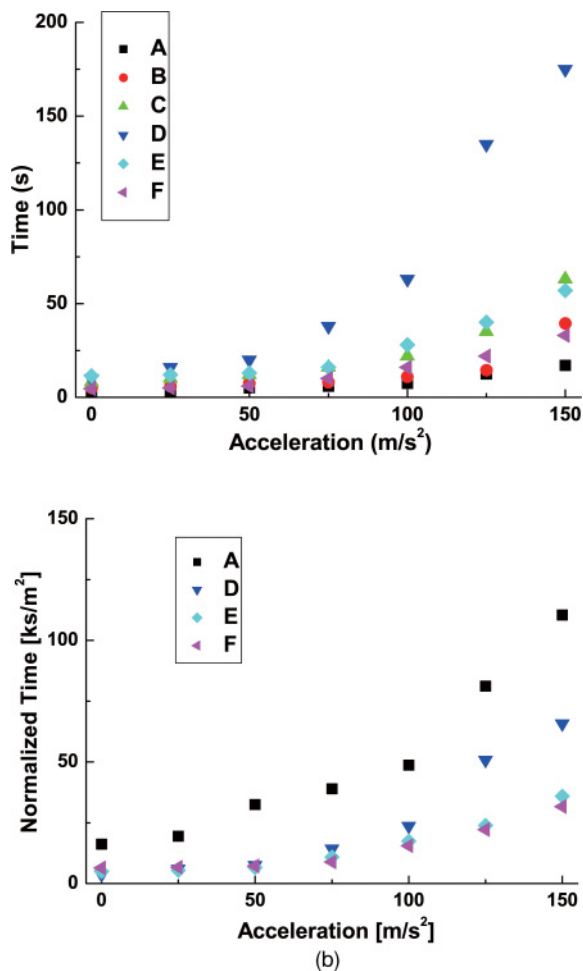


FIG. 9. (Color online) (a) Time required to disappear for the initial hole produced by different shapes and sizes of rubber plugs versus acceleration for sample with the volume fraction 50% at 40 Hz. (b) Normalized time by hole area versus acceleration in the same situation.

the effect of the initial hole shapes, the disappearing time would be normalized by hole area. There are four kinds of shapes used here, including the round shape A, the hexagonal shape D, the cross shape E, and the flat blade shape F. The normalized time versus acceleration is shown in Fig. 9(b). By comparing data A with data B, the influence of the round initial hole's diameter on the disappearing time could be obtained, and a longer disappearing time is needed for the initial hole with a large diameter than that with a small one. Especially, when the acceleration becomes large, the STF sample exhibits shear thickening effect, and the difference of disappearing times for holes with different diameters becomes obvious. Rubber plugs C and E are both cross shape and different in the length of branch. There are few differences between the two sets of data (data C and data E), which indicates the length of branch does not affect the disappearing time. At the end, the branch disappears immediately in the period of disappearance of the hole. The time required for the hole to disappear is mainly determined by the disappearing time for the central part. This will be verified by comparing data D, data E, and data F. With increasing the branch's number, the

area of the central part increases. Similarly, in comparison of data A with data B, the larger the area of the central part is, the longer the disappearing time is required. Among D, E, and F, the normalized time for the hexagonal shape D is the largest at the same acceleration. The larger the branch's number is, the larger the area of the central part is and the more concentrated the shape's distribution is. Therefore, the shape's distribution is important to the normalized time. As the shape's distribution becomes concentrated, the normalized time becomes long. When the shape's distribution becomes the most concentrated, the shape transforms into a circle, which is shown in Fig. 9(b) as data A. It is demonstrated that data A has the most concentrated shape's distribution and the largest normalized time. From the above discussion, the disappearance for the central part principally contributes to the whole initial hole's disappearance regardless of the branches.

### C. Fission of the hole

For the low volume fraction sample, no fission is observed in the experimental range of the testing acceleration. For the high volume fraction sample, when the acceleration exceeds a certain threshold, fission of the initial hole occurs. Figure 10 shows the evolution of the fission of the initial hole at 225 and 250 m s<sup>-2</sup>, respectively. It can be seen from Figs. 10(a) and 10(d) that a circle of the protuberance appears at the edge of the hole due to a strong convection. Parts of protuberance may fall into the hole, and then the parts may disappear at the bottom of the hole, or separate the hole into small holes. Similarly, the small holes in the other figure also have convections at their edges, and they will still divide and spread. The small holes adjust their own size according to the applied acceleration.

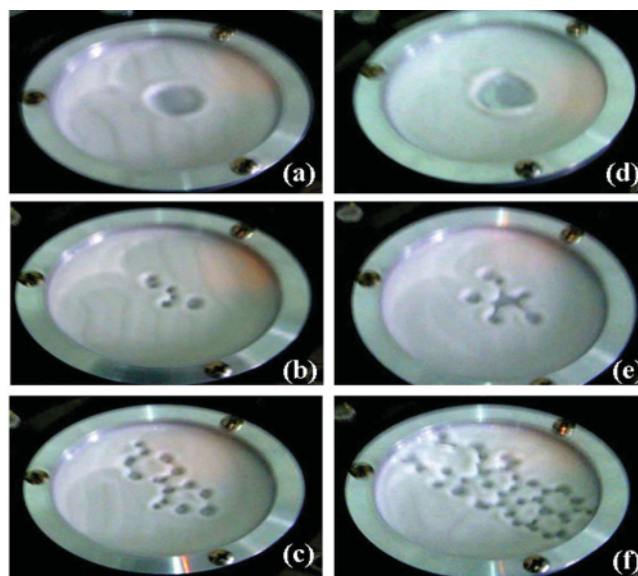


FIG. 10. (Color online) Evolution of the fission of the initial hole produced by rubber plug B for sample with the volume fraction 60% at 40Hz. (a)  $a = 225 \text{ m s}^{-2}$ ,  $t = 0 \text{ s}$ ; (b)  $a = 225 \text{ m s}^{-2}$ ,  $t = 20 \text{ s}$ ; (c)  $a = 225 \text{ m s}^{-2}$ ,  $t = 140 \text{ s}$ ; (d)  $a = 250 \text{ m s}^{-2}$ ,  $t = 0 \text{ s}$ ; (e)  $a = 250 \text{ m s}^{-2}$ ,  $t = 10 \text{ s}$ ; (f)  $a = 250 \text{ m s}^{-2}$ ,  $t = 60 \text{ s}$ .

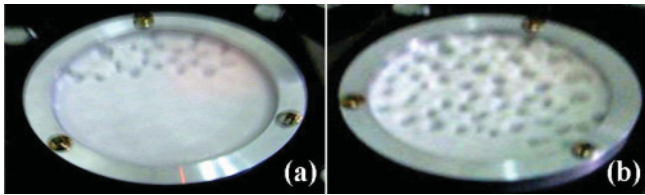


FIG. 11. (Color online) Disorder state for sample with the volume fraction 60% at 40 Hz and  $290 \text{ m s}^{-2}$ . (a) Without the initial hole; (b) with the initial hole.

In the process of spreading, the arrangement of small holes has a certain pattern. As shown in Figs. 10(c) and 10(f), the pattern of holes is similar to the hexagonal self-organized arrangement. Because of a weak attractive interaction two simultaneous holes drift toward each other and keep a finite distance, which is similar to the previously report [27]. The as-formed self-assembly structures are similar to the crystalline pattern. After 140 s vertical vibration, the surface of the STF sample at a low acceleration ( $225 \text{ m s}^{-2}$ ), displays only two hexagons. In contrast, large numbers of hexagons can be found in the surface of STF sample after 60 s vertical vibration is conducted, when a relative high acceleration ( $250 \text{ m s}^{-2}$ ) is applied. Consequently, the rate of fission and spreading are directly depended on the acceleration. When the acceleration increases, the rate of fission and spreading becomes fast. The weak attractive interaction becomes strong, and the stabilized finite distance apart between two holes becomes small. Therefore, both the size of the hexagonal arrangement and the diameter of the small holes decrease with increasing the acceleration.

To date, the patterns of vertically vibrated STF observed include the persistent hole [10], the expanding hole [11], and so on. However, the spontaneous hexagonal arrangement is a particular pattern that is not found in other literature. Moreover, due to the limitation of our vibration test system, at a relative high frequency or a relative low frequency, the fission of the initial hole, which needs a high acceleration or large displacement amplitude, could not be observed in the present work. Therefore, this spontaneous hexagonal pattern is worthy of further investigation.

#### D. Disorder state

Similar to other literature [10,11], when the acceleration reaches a certain value, the surface of the vertically vibrated high volume fraction sample presents an irregularly disordered state (shown in Fig. 11). Regardless of the existence of the initial hole, the disorder state will appear above a certain value.

In our experiment, the value is  $290 \text{ m s}^{-2}$  at 40 Hz. If there is no initial hole, a small hole will be generated first in the interface between the wall and the surface of suspension. The cohesion in the interface is the weakest at the surface of suspension, and thus the suspension is torn from the wall and the small hole appears. Then the small hole begins to be divided and spread randomly. If the initial hole exists, the fission and spreading take place synchronously. In addition, the new hole in the interface needs enough time to come into being by tearing from the wall. Therefore, at the same time the surface of STF sample with the initial hole has smaller holes than that without the initial hole. Obviously, these results will provide more evidence for investigation of vertically vibrated STF.

#### IV. CONCLUSIONS

The experiments show that a vertically vibrated concentrated suspension of PMMA particles suspended in ethylene glycol displays the following types of surface instability: disappearance of the hole, fission of the hole, and disorder state. The evolution of the initial hole in vertically vibrated shear thickening fluids could be explained by the convection-like flow at the rim of the hole. During the disappearance of the hole, a simplified model is employed to analyze the influencing factors. These patterns are obtained by the introduction of a finite perturbation. At low acceleration, the analysis results indicate that acceleration, frequency, volume fraction, thickness, and the initial hole's shape and size play an important role in the disappearance of the hole. The acceleration, volume fraction, and area of the hole's central part are proportional to the disappearing time. Meanwhile, the frequency is inversely proportional to the disappearing time. The influence of thickness is dependent on the forcing acceleration. At a higher acceleration the initial hole becomes unstable and begins to split to form a hexagonal arrangement. Results suggest that the size of the hexagonal arrangement and the diameter of the small holes both become small with increasing acceleration. At even higher acceleration, the surface transforms to a disorder state. More experiments and theories will be in progress to further elucidate the relationship between the surface instability of suspension and rheological property.

#### ACKNOWLEDGMENTS

Financial support from the National Basic Research Program of China (973 Program, Grant No. 2007CB936800) is gratefully acknowledged.

- [1] H. A. Barnes, *J. Rheol.* **33**, 329 (1989).
- [2] S. Raghavan and S. Khan, *J. Colloid Interf. Sci.* **185**, 57 (1997).
- [3] B. J. Maranzano and N. J. Wagner, *J. Chem. Phys.* **114**, 10514 (2001).
- [4] B. J. Maranzano and N. J. Wagner, *J. Rheol.* **45**, 1205 (2001).
- [5] Y. S. Lee and N. J. Wagner, *Rheol. Acta* **42**, 199 (2003).
- [6] I. S. Aranson and L. S. Tsimring, *Rev. Mod. Phys.* **78**, 641 (2006).

- [7] A. Barrat and E. Trizac, *Phys. Rev. E* **66**, 051303 (2002).
- [8] N. J. Wagner and J. F. Brady, *Phys. Today* **62**, 27 (2009).
- [9] E. Brown, N. A. Forman, C. S. Orellana, H. J. Zhang, B. W. Maynor, D. E. Betts, J. M. Desimone, and H. M. Jaeger, *Nat. Mater.* **9**, 220 (2010).
- [10] F. S. Merkt, R. D. Deegan, D. I. Goldman, E. C. Rericha, and H. L. Swinney, *Phys. Rev. Lett.* **92**, 184501 (2004).

- [11] H. Ebata, S. Tatsumi, and M. Sano, *Phys. Rev. E* **79**, 066308 (2009).
- [12] P. Melby, F. V. Reyes, A. Prevost, R. Robertson, P. Kumar, D. A. Egolf, and J. S. Urbach, *J. Phys.: Condens. Matter* **17**, 2689 (2005).
- [13] M. Faraday, *Philos. Trans. R. Soc. London* **121**, 299 (1831).
- [14] G. I. Taylor, *Proc. R. Soc. London Ser. A* **201**, 192 (1950).
- [15] P. Umbanhowar, F. Melo, and H. L. Swinney, *Nature (London)* **382**, 793 (1996).
- [16] P. Ballesta and S. Manneville, *Europhys. Lett.* **76**, 429 (2006).
- [17] O. Lioubashevski, Y. Hamiel, A. Agnon, Z. Reches, and J. Fineberg, *Phys. Rev. Lett.* **83**, 3190 (1999).
- [18] J. M. Schleier-Smith and H. A. Stone, *Phys. Rev. Lett.* **86**, 3016 (2001).
- [19] R. D. Deegan, *Phys. Rev. E* **81**, 036319 (2010).
- [20] H. Shiba, J. E. Ruppert-Felsot, Y. Takahashi, Y. Murayama, Q. Ouyang, and M. Sano, *Phys. Rev. Lett.* **98**, 044501 (2007).
- [21] T. Epstein and R. D. Deegan, *Phys. Rev. E* **81**, 066310 (2010).
- [22] W. Q. Jiang, Y. Q. Sun, Y. L. Xu, C. Peng, X. L. Gong, and Z. Zhang, *Rheol. Acta* **49**, 1157 (2010).
- [23] W. H. Li, H. J. Du, and N. Q. Guo, *Mater. Sci. Eng. A* **371**, 9 (2004).
- [24] W. H. Li, H. J. Du, G. Chen, S. H. Yeo, and N. Q. Guo, *Rheol. Acta* **42**, 280 (2003).
- [25] Y. L. Xu, X. L. Gong, C. Peng, Y. Q. Sun, W. Q. Jiang, and Z. Zhang, *Chin. J. Chem. Phys.* **23**, 342 (2010).
- [26] D. P. Kalman, R. L. Merrill, N. J. Wagner, and E. D. Wetzel, *ACS Appl. Mater. Interf.* **1**, 2602 (2009).
- [27] S. Protiere, A. Boudaoud, and Y. Couder, *J. Fluid Mech.* **554**, 85 (2006).